Direct numerical simulation of transitions towards structural vacillation in an air-filled, rotating, baroclinic annulus

Peter L. Read, Pierre Maubert, Anthony Randriamampianina, Wolf-Gerrit Früh

Direct numerical simulation of transitions towards structural vacillation in an air-filled, rotating, baroclinic annulus

Peter L. Read,[1,a)] Pierre Maubert,[2] Anthony Randriamampianina,[2] and Wolf-Gerrit Früh[3]
[1]*Atmospheric Oceanic and Planetary Physics, Department of Physics, Clarendon Laboratory, Parks Road, Oxford OX1 3PU, United Kingdom*
[2]*Institut de Recherche sur les Phénomènes Hors Equilibre, UMR 6594 CNRS, Technopôle de Château-Gombert, 49, rue Frédéric Joliot-Curie, BP 146, 13384 Marseille Cedex 13, France*
[3]*School of Engineering Physical Sciences, Heriot-Watt University, Riccarton, Edinburgh EH14 4AS, United Kingdom*

(Received 6 May 2007; accepted 11 March 2008; published online 25 April 2008)

The route to chaos of baroclinic waves in a rotating, stratified fluid subjected to lateral heating can occur via several possible routes, involving either low-dimensional, quasiperiodic states or via a series of secondary small-scale instabilities. In a recent paper, we have discussed direct numerical simulations (DNS) of the low-dimensional route to chaos in a baroclinic annulus filled with air as the working fluid and compared results to those obtained in the laboratory for high Prandtl number liquids. In the present paper, we consider further DNS in the air-filled annulus at higher rotation rates. A transition in the flow structure is observed, where the centrifugal acceleration exceeds gravity and the dominant physical process changes from baroclinic instability to convection due to radial buoyancy. The transition of this convection to chaotic behavior is fundamentally different from that observed in the transition to the chaotic flow observed at lower rotation rates. Rather than via a sequence of low-dimensional, quasiperiodic states, the large-scale convection developed small-scale instabilities, which has been previously suggested as the origin of structural vacillation on the transition to geostrophic turbulence. © *2008 American Institute of Physics*.
[DOI: 10.1063/1.2911045]

I. INTRODUCTION

The transition to disordered behavior in the form of "baroclinic chaos" provides an important prototypical form of chaotic transition in fluid dynamics. This is of particular geophysical relevance in the context of understanding the origins of chaotic behavior and limited predictability in the large-scale atmospheres of the Earth and other terrestrial planets, such as Mars, and in the oceans.[1–3] For many years, the differentially heated, rotating cylindrical annulus has proven a fruitful means of studying the properties of fully developed, nonlinear forms of baroclinic instability in the laboratory. Laboratory measurements have enabled various aspects of its time-dependent behavior to be studied under a variety of conditions. Some have operated in a range where the Coriolis acceleration was the main factor affecting the flow, whereas the centrifugal acceleration only resulted in a small, or moderate at most, modification of the isopotentials.[4–9] Others operated at much higher rotation rates, where the centrifugal term was stronger than gravity, effectively resulting in radial buoyancy.[10–13] The system is well known to exhibit a rich variety of different flow regimes, depending on the imposed conditions (primarily the temperature contrast ΔT and rotation rate Ω), ranging from steady, axisymmetric circulations through highly symmetric, regular wave flows to fully developed geostrophic turbulence.

Extensive experimental studies of transitions to chaotic behavior in the laboratory[8,9] have demonstrated that the onset of chaotic behavior could take place via at least two different types of transition sequences. The first of these was via a quasiperiodic route, in which a periodic amplitude-modulated wave ("amplitude vacillation") develops secondary modulation at a long period, typically involving the instability of a nonharmonic azimuthal sideband mode. The onset of this secondary modulation was typically found to be chaotic (from computation of the largest Lyapunov exponent), except when the modulation frequency was commensurate with the spatial drift frequency. An exception to this rule was found by Randriamampianina *et al.*[14] who observed a quasiperiodic modulated amplitude vacillation of a wave with azimuthal mode $m=2$ in an otherwise classic bifurcation sequence of three Hopf bifurcations. An alternative to the classical Ruelle–Takens quasiperiodic route indicated above is a torus-doubling route which, for example, has been observed in some two-layer baroclinic experiments,[15,16] though seems to have been elusive so far in the thermally driven annulus. At higher rotation rates, the route to disorder appears to emerge via a rather different mechanism involving small-scale secondary instabilities, possibly leading to the growth of higher order radial mode baroclinic waves[5,17] or barotropic instabilities. This is, in a manner, reminiscent of the classical instability of Rossby waves.[18,19] At intermediate parameter values, this can lead to the wave pattern appearing to change its orientation or structure in a roughly periodic fashion, in a form known as "tilted trough" or "structural

a)Author to whom correspondence should be addressed. Electronic mail: p.read1@physics.ox.ac.uk.

vacillation" (SV). In other circumstances, the parameters of which are not well understood, a large-scale wave flow may develop irregular, small-scale secondary instabilities or eddies, which lead to erratic modulations of the large-scale pattern.[7]

Such a sequence of transitions via structural vacillation seems to lead rapidly to the development of a complex, time-dependent flow of relatively high attractor dimension,[8,20] well before the spatial flow pattern appears obviously disordered. Subsequent development within this so-called "transition zone" as Ω is further increased[6] leads to the gradual and progressive breakdown of the initially regular wave pattern into an increasingly disordered flow, ultimately leading to the emergence of a form of stably stratified "geostrophic turbulence." The latter is another important paradigm in geophysical fluid dynamics, with properties which may markedly differ from the well known homogeneous, isotropic turbulence in three dimensions, more closely resembling those of idealized two-dimensional turbulence under some circumstances.[3,21]

In a companion paper,[14] we have presented and discussed a set of direct numerical simulations (DNSs) which exhibit in detail a transition to baroclinic chaos via a low-dimensional route involving a succession of modulated traveling waves in an air-filled, rotating annulus. Such studies complement the use of analytical and numerical stability and continuation methods in the context of circularly symmetric systems such as the rotating annulus,[22–27] though the latter approaches are not yet able to deal with the full complexity of time-dependent, modulated waves and their nonlinear interactions found in the present work. The use of air as the working fluid is of particular interest since this represents a fluid with Prandtl number Pr=O(1) which has received relatively little attention in previous experimental studies[28] or in numerical simulations of baroclinic flows but, in common with other convective flows, the Prandtl number seems to play an important role in governing the nature of nonlinear interactions in the flow, as well as strongly affecting the form of the advective-diffusive basic state from which baroclinic instabilities grow. This evidently leads to significant variations in the type and order of bifurcations in the low-dimensional route to chaos, depending on the value of Pr.[14,29] In particular, it has been noted that amplitude vacillation was significantly more widespread at high Prandtl number, though the onset of "structural vacillation" close to the transition zone at high Taylor number was less sensitive to Pr.[30]

In the present paper, we extend our earlier study in an air-filled annulus to cover a range of parameter space in which a wavenumber $m=3$ baroclinic wave undergoes a series of transitions to a form of structural vacillation. This study includes a range in rotation rate of the annulus where the centrifugal term was no longer small but in the range between the paradigms of Hide and Mason[4] and of Busse and Carrigan.[10] As was seen in both idealized models and earlier experiments in high Pr liquids, the large-scale wave is found to undergo qualitative flow transitions, leading to the appearance of additional spatial modes with more complex radial structure than the initial flow, associated with the onset of rapid time-dependent fluctuations. This is characterized by using a variety of diagnostics, as outlined below, and compared to measurements and simulations in other baroclinic systems.

The model is summarized in Sec. II, together with a brief description (in Sec. III) of the main techniques used to analyze the data from the simulations. Section IV presents the results, including an overview of the main regimes observed and detailed discussions of the flows encountered from $m=3$ toward either quasiperiodic amplitude vacillation or structural vacillation via a mixed vacillation regime not previously identified in other work. The overall results are discussed in the light of previous work and wider issues in Sec. V.

II. THE NUMERICAL MODEL

The model is described in detail by Randriamampianina *et al.*[14] and so is only briefly summarized here. The physical model comprises a body of air contained between two vertical, coaxial cylinders held at constant temperatures and two horizontal insulating rigid endplates separated by a distance of d. The whole cavity rotates at a uniform rate, where the rotation vector $\mathbf{\Omega}=\Omega\mathbf{e}_z$ is antiparallel to the gravity vector $\mathbf{g}=-g\mathbf{e}_z$ and coincides with the axis of the cylinders. The inner cylinder at radius $r=a$ is cooled (T_a) and the outer cylinder at radius $r=b$ is heated ($T_b>T_a$), thus imposing a temperature difference $\Delta T=T_b-T_a$ across the annular gap of width $L=b-a$.

The geometry is defined by an aspect ratio, $A=d/L=3.94$ and a curvature parameter, $R_c=(b+a)/L=3.7$, corresponding to the configuration used by Fowlis and Hide[31] in their experiments with liquids with $a=34.8$ mm, $b=60.2$ mm, and $d=100$ mm. The working fluid is air at ambient temperature $T_0=293$ K, with a kinematic viscosity of $\nu=1.697\times10^{-5}$ m^2/s and a thermal diffusivity of $\kappa=2.400\times10^{-5}$ m^2/s so that Pr=0.707. By using the thermal expansion coefficient for an ideal gas of $\alpha=1/T_0$, where $T_0=(T_a+T_b)/2$, the fluid can still be assumed to satisfy the Boussinesq approximation, with constant properties except for the density when applied to the Coriolis, centrifugal, and gravitational accelerations, for which $\rho=\rho_0[1-\alpha(T-T_0)]$.

The model variables are nondimensionalized by using reference scales for the velocity of $g\alpha\Delta T/(2\Omega)$ and for the time of $(2\Omega)^{-1}$. The dimensionless temperature is defined by $2(T-T_0)/\Delta T$. The overall motion is governed by the following dynamic parameters: the Prandtl number $\mathrm{Pr}=\nu/\kappa$, the Rayleigh number $\mathrm{Ra}=g\alpha\Delta TL^3/(\nu\kappa)$, a Froude number $\mathrm{Fr}=\Omega^2L/g$, and the Taylor number,

$$\mathrm{Ta}=\frac{4\Omega^2L^5}{\nu^2d}. \tag{1}$$

Following a long-established tradition,[4,31] the analysis of the flow for a given fluid in a fixed geometry is made by varying two main parameters: the Taylor number Ta and the thermal Rossby or Hide number,

$$\Theta = \frac{gd\alpha\Delta T}{\Omega^2 L^2} \equiv \frac{4\mathrm{Ra}}{\mathrm{PrTa}}. \tag{2}$$

The thermal Rossby or Hide number can be interpreted twofold, as a Rossby number, where it is the ratio of the inertial terms over the Coriolis term using the thermal wind as the velocity scale, or as a measure of the stability of the thermal stratification in relation to the Brunt–Väisälä frequency and the Coriolis parameter $f=2\Omega$. As such it is related to a rotational Froude number defined for internal waves. The Froude number introduced above relates the centrifugal acceleration to that of gravity. In buoyancy driven flows, natural convection is expected to dominate at small values of the Froude number, whereas the radial centrifugal acceleration will drive the convection at large Fr. While the gap width is an obvious choice as the reference length scale in the definition of this dimensionless parameter, the actual ratio between the two forces resulting in buoyancy is given by the radial distance from the axis of rotation,

$$\mathrm{Fr}_r = \frac{\Omega^2 r}{g}, \tag{3}$$

which depends on the position in the annulus. For some analyses, the observations were related to this local Froude number evaluated at three key points, namely, at the inner radius: Fr_a with $r=a$, at the center of the gap: Fr_c with $r=(a+b)/2$, and at the outer radius: Fr_b with $r=b$.

The model equations are solved by using a pseudospectral collocation-Chebyshev and Fourier method, in which each dependent variable is expanded in the r- and z-directions by using Chebyshev polynomials of degrees less than or equal to N and M, respectively, while Fourier series to a mode J are used to represent variables in the azimuthal direction. The time integration used is second order accurate and is based on a combination of Adams–Bashforth and backward differentiation formula schemes, chosen for its good stability properties.[32] Various grid resolutions, ranging from $N\times M\times J=80\times 96\times 64$ to $N\times M\times J=108\times 108\times 256$ for the radial, axial, and azimuthal components, respectively, were used and corresponding values of time step to stay within the numerical stability limit. The detailed accuracy of the numerical techniques used here has been discussed by Raspo *et al.*,[33] who noted that insufficient mesh resolution primarily leads to an incorrect pressure field and a velocity field that is not divergence-free. In the present work, therefore, careful checks were made on the norm of the velocity divergence at the boundaries to ensure that the solutions were reliable. In addition, care was taken to test for convergence in time of each solution, especially for steady and quasiperiodic flows. Although there is some small, residual "roughness" apparent in some of the contour figures shown below, these are not thought to indicate significant inaccuracies in the numerics.

The strategy for the investigation usually consisted of progressively increasing the rotation while keeping the temperature difference fixed. To explore solutions found after a transition with hysteresis, some integrations were also carried out after decreasing the rotation rate. This strategy largely follows long-established practice in laboratory experimentation and was found to be an effective means of following the stability and transitions in the regular and weakly chaotic baroclinic wave regimes around $m=2$ in our earlier study,[14] some aspects of which have since been verified in the laboratory.[28]

III. DATA ANALYSIS

As in our companion study, for a number of diagnostics the three-dimensional velocity, pressure, and temperature fields were reduced to two-dimensional sections, to the radial-vertical fields of the azimuthally averaged quantities, and also to one-dimensional sections around the azimuth at a given radius and height in the annulus. These sections gave the temporal evolution of the set of azimuthal Fourier modes, which could then be used to calculate instantaneous or time-averaged spatial wavenumber spectra and a temporal power spectrum of a particular Fourier mode or wave amplitude.

Attractor reconstruction methods were also used in forms similar to those used in our companion study, either directly from the (complex) amplitudes of various azimuthal Fourier modes or via various univariate or multivariate embedding techniques based on the method of delays and/or singular value decomposition or singular systems analysis.[34]

The spatial structure especially associated with the onset of structural vacillation is of particular interest, since it may be associated with qualitative flow transitions involving quite different spatial modes. As a means of isolating the dominant patterns in the flow, we have made use of a form of empirical orthogonal function (EOF) analysis,[35] in which time sequences of spatial maps, e.g., of temperature at midheight, were analyzed to obtain the covariance matrix of every spatial point with every other in the two-dimensional field.

The eigenvectors of such a covariance matrix represent an optimal basis of mutually orthogonal spatial patterns contributing to the variance of the flow, while the eigenvalues represent the magnitude of the relative contribution of the corresponding eigenvalue to the total variance. In the present cases, a sequence of two-dimensional horizontal temperature fields in (r,θ) at midheight was analyzed, sampled in time at intervals of one per dimensionless time unit (much larger than the numerical timestep, see Ref. 14) to represent the variability exhibited by the flow at a rate corresponding to approximately 20–40 samples per drift period of the dominant wave pattern. The eigenvalues and eigenvectors were then computed from the resulting real, symmetric covariance matrix by using Householder reduction and QL decomposition (via the EIGENQL routine of IDL).

IV. RESULTS

The presentation of the results is broadly divided into four sections, beginning with an overview of the flow types observed in the parameter space spanned by the two parameters, Ta and Θ, which puts our results into context with the previous studies. The second part introduces the new results in terms of their typical structure and spectral properties. This is then followed by a detailed analysis of the structure of the steady waves which demonstrate a change of dynam-

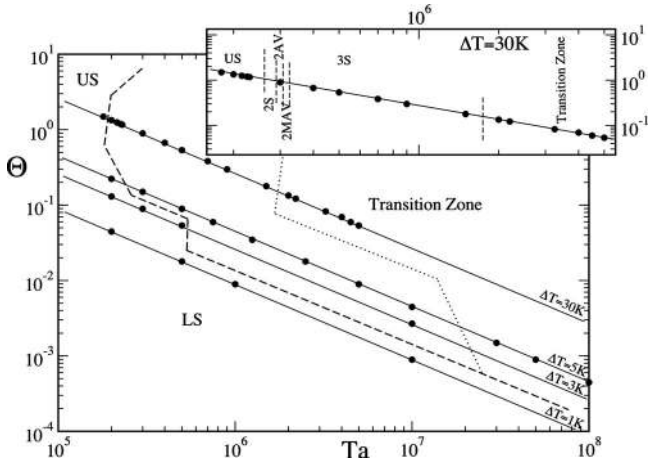

FIG. 1. Summary of the regimes for air with Prandtl number of 0.7 as obtained by the numerical model. The solid lines represent paths in which Ω varies at constant temperature difference; individual simulations were carried out as identified by the dots. The dashed line indicates the approximate location of the transition from axisymmetric flow to regular waves, while the dotted line separates the regular waves from the transition zone, representing the onset of irregular behavior. The inset is a more detailed closeup of the path at $\Delta T=30$ K where the main regimes and transitions between them are indicated.

ics following the increasing importance of the centrifugal term. Finally, the time-dependent flows are presented in detail.

A. Overview of observed regimes

The basic regimes observed in the present sequence of simulations are summarized in Fig. 1, many of the details of which were discussed in our companion paper.[14] The regime diagram in Fig. 1 is a compilation of results from this study as well as previous studies with this model and configuration.[14,36] Maubert and Randriamampianina[36] covered the smaller temperature differences of $\Delta T \leqslant 5$ K. The dashed line, which identifies the approximate position of the transition from the axisymmetric flow to traveling waves, reproduces the well known "anvil" shape,[37] with the distinction between the viscously stabilized "lower symmetric" regime and the stably stratified "upper symmetric" regime. The dotted line suggests a transition from regular waves to more irregular flow which, while still dominated by large-scale wave modes, would ultimately lead to geostrophic turbulence. The range in between these two lines is where regular waves can be found, whose wave number tends to be lower at larger values of Θ and, conversely, higher at smaller values of Θ up to a geometrically constrained upper limit, which is $m \approx 8$ in the present geometry.[36] Several stable solutions of different wave numbers may coexist in many regions of parameter space, which leads to widespread and substantial hysteresis in transitions between flows of different wave numbers.

The more recent studies addressed the traverse at $\Delta T = 30$ K which is shown in the enlarged inset in Fig. 1, where the earlier companion paper discussed mainly the dynamics of the $m=2$ regimes. At the lowest values of rotation rate or Taylor number, only the "upper axisymmetric" solution was found. This then bifurcated in a subcritical Hopf bifurcation with an associated saddle node to a wave solution of azimuthal wave number $m=2$ with a steady wave amplitude. In two successive supercritical Hopf bifurcations, this solution developed first a periodic oscillation, known as amplitude vacillation, 2AV, then a quasiperiodic modulated amplitude vacillation, 2MAV, which finally became chaotic. This solution branch of the $m=2$ solutions is discussed in detail by Randriamampianina *et al.*[14] Two main points from that report were, first, that laboratory flows in liquids at higher Prandtl numbers, $\mathrm{Pr} \gtrsim 7$, show a reversed sequence for the onset of AV on decrease of Taylor number and, second, that the third Hopf bifurcation did not directly lead to chaotic flow but first led to a quasiperiodic flow with three free and incommensurate frequencies, which became chaotic in a global bifurcation only after a finite increase in the control parameter.

As has already been mentioned, the branch of the $m=2$ solutions was abruptly terminated at a Taylor number of $\mathrm{Ta} = 230{,}000$, where the solution exhibited an exchange of stabilities and equilibrated to a steady wave of azimuthal wave number $m=3$. The focus of this paper is the extension of that study to much higher values of Taylor number and a detailed analysis of the behavior of that $m=3$ solution branch.

B. The wavenumber three flows and their horizontal structure

Figure 2 shows the equilibrated amplitude of the dominant azimuthal mode against the Taylor number. For steady solutions, the equilibrated amplitude of that wave mode is shown, while for time-dependent solutions, the maximum and minimum as well as the mean amplitude are given. As such, the figure is a schematic "pseudobifurcation diagram," in which lines connecting different solutions have been interpolated to suggest plausible solution branches and represent the sequence of three basic solutions, the axisymmetric solution (labeled "0") on the x-axis and the $m=2$ and $m=3$ solutions (labeled "2" and "3") projected onto the same plane. The instability of the axisymmetric solution and the $m=2$ solution branch are reproduced from the earlier study.[14] Continuing the evolution of the solution types on increasing the Taylor number, at $\mathrm{Ta} = 0.23 \times 10^6$, the chaotic 2MAV was replaced by a steady flow of azimuthal wavenumber $m=3$ in a mode transition, as is illustrated in Fig. 2. This mode transition showed substantial hysteresis, as is commonly found in the baroclinic annulus and, by successively reducing the Taylor number, the steady $m=3$ could be followed as far as $\mathrm{Ta} = 0.2 \times 10^6$ before losing stability to $m=2$.

As will be discussed in detail in Sec. IV C, the three-dimensional structure of the flow responds to a shift in the balance between gravity and the centrifugal acceleration, quantified by the Froude number, Eq. (3). $\mathrm{Fr}_a > 1$ implies that the centrifugal acceleration is larger than gravity everywhere in the fluid. This ratio was used as the secondary axis on top of the graph in Fig. 2 and the location of $\mathrm{Fr}_a = 1$ is highlighted by the dotted vertical line at Ta=414 000. The first vertical line, at Ta=239 000, indicates where the centrifugal acceleration equals gravity at the outer cylinder, $\mathrm{Fr}_b = 1$. Below that Froude number or Taylor number, gravity is the

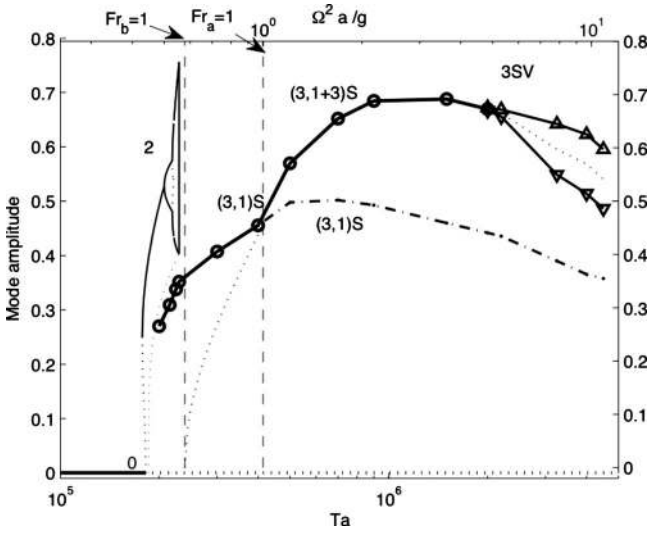

FIG. 2. Summary of the regimes obtained by the numerical model for a temperature difference of $\Delta T=30$ K, in the form of a schematic "pseudobifurcation diagram." For steady solutions, the equilibrated amplitudes of the dominant solution is shown, while for time-dependent solutions the amplitude range of that mode is shown. The axis at the bottom shows the Taylor number while the axis at the top shows the ratio of the centrifugal term to gravity at the inner radius. The horizontal solid line, labeled "0," denotes the stable axisymmetric solution, while the curve labeled "2" summarizes the solution branch dominated by the wavenumber $m=2$ flow discussed by Ref. 14. The line with the open circles represents the steady $m=3$ solution, comprising either the lowest radial mode of the azimuthal mode $m=3$ $[(3,1)S]$ or a superposition of the first and third radial modes of that wave $[[3,1+3]S]$. The lines with the triangles denote the maxima and minima of the amplitude variation of the mixed mode $(3,1+3)$, labeled as "3SV." The dotted lines are suggested curves of unstable branches, indirectly inferred from the observed stable branches. The vertical dashed lines indicate where the local Froude number is unity at the outer radius ($\mathrm{Fr}_b=1$ at $\mathrm{Ta}=239\,000$) and at the inner radius ($\mathrm{Fr}_a=1$ at $\mathrm{Ta}=414\,000$), respectively.

stronger of the two forces everywhere in the annulus, as is the case for the entire $m=2$ solution branch. It can be seen that $\mathrm{Fr}_a=1$ corresponds to a place on the solution branch where the radial structure of the steady wave changes. Describing the horizontal flow structure in terms of azimuthal and radial modes, this corresponds to a qualitative transition below which the flow is largely described by the first radial mode of a traveling wave with azimuthal wave number three. For that flow, the wave signature is fairly broad and strongest in the center of the annulus. At the transition, a higher radial mode of the same azimuthal wave grows to a finite amplitude while the first radial mode appears saturated and even decays. This results in an increasing concentration of the wave signature nearer the side walls, which is eventually visible as one or two very narrow wave trains near each side boundary.[14] This growth of the higher radial modes, or the concentration of the waves near the boundaries, continues at first, but then saturates in the region of $\mathrm{Ta}\sim 10^6$. In terms of the physical quantities, this development results in strong velocity and temperature gradients near the boundaries and the concentration of the radial transport of heat and momentum into narrow plumes or jets as illustrated by the maps of the temperature and horizontal velocity vectors in a horizontal plane at midheight in Fig. 3.

The basic horizontal flow pattern of the $m=3$ flow is illustrated in Fig. 3, which displays maps in the (r,θ) plane of temperature and velocity vectors at midheight in the annulus for typical $m=3$ cases at $\mathrm{Ta}=2.35\times 10^5$ [(a) and (d)], 5×10^5 [(b), and (e)] and 1.5×10^6 [(c) and (f)], traversing the transition from flows dominated by normal gravity to those dominated by radial centrifugal buoyancy. As Ta is increased, the temperature fields show the increased presence

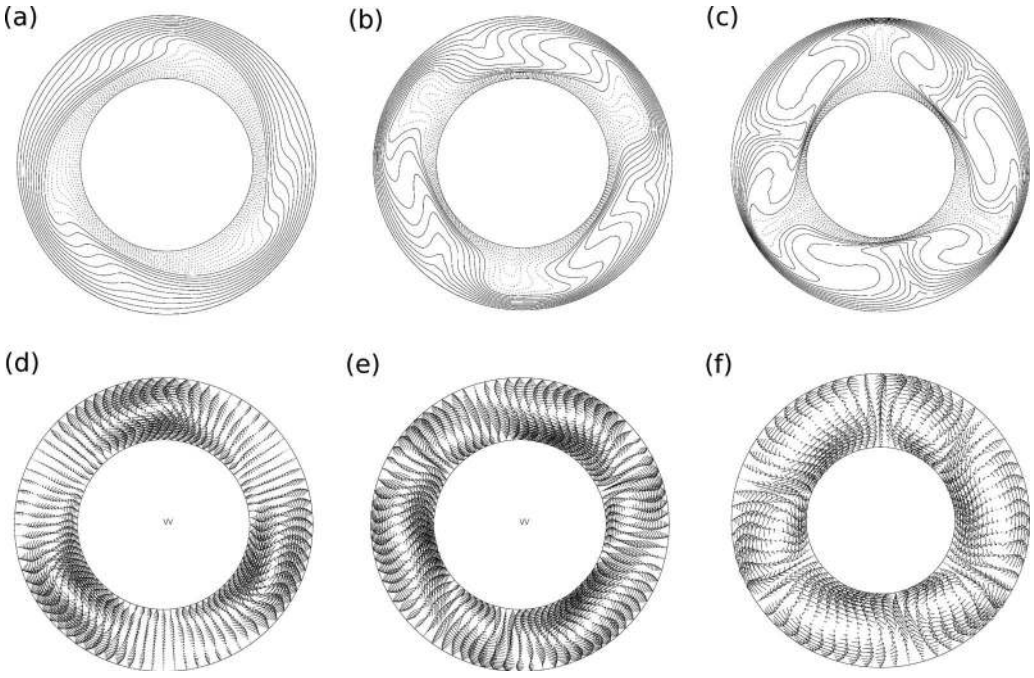

FIG. 3. Maps of temperature (a)–(c) and velocity vectors (d)–(f) in typical wave-3 flows at $\mathrm{Ta}=2.35\times 10^5$ [(a) and (d)] 5×10^5 [(b) and (e)], and 1.5×10^6 [(c) and (f)] in a horizontal plane at midheight.

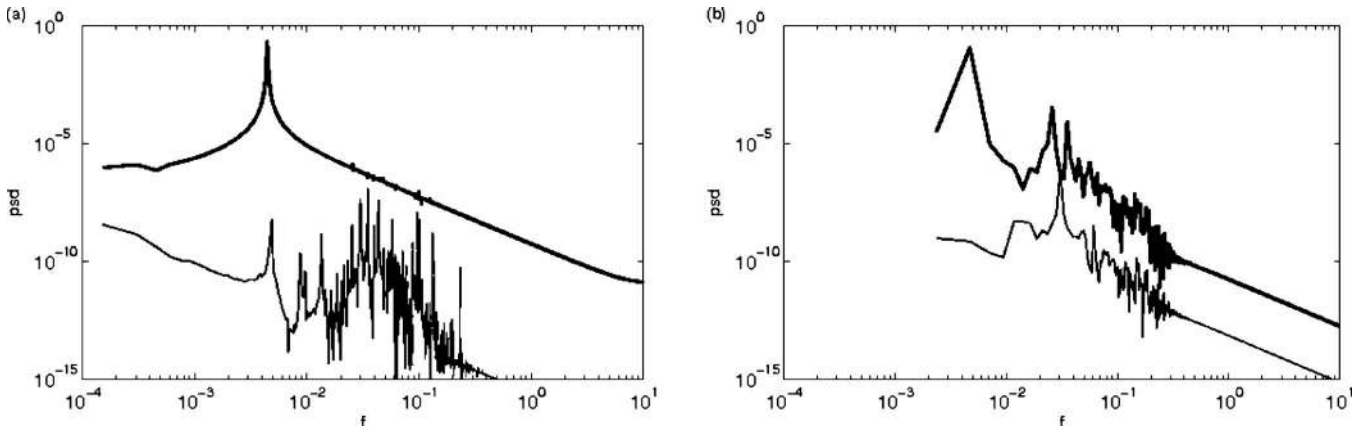

FIG. 4. Temporal spectra of mode $m=3$ for Taylor numbers (a) $\mathrm{Ta}=2\times10^6$ and (b) 3.25×10^6. The upper spectrum in each figure is of the cosine component of mode 3, while the lower spectrum in the same frame is of the amplitude of mode 3. The amplitude spectrum in (b) was divided by a factor of 100 to separate it from the cosine spectrum.

of pronounced plumes alternately of warm and cool airs, highly concentrated in azimuth and crossing the annular gap radially in association with strong radial jets apparent in the velocity fields. Such highly concentrated structures become much more apparent at the highest rotation rates [see Figs. 3(c) and 3(f)].

At the highest values of Taylor numbers explored, between 2 and 5×10^6, that flow then developed temporal fluctuations. Unlike the sequence of Hopf bifurcations on the $m=2$ branch at much lower values of Ta or Fr_a, however, no quasiperiodic vacillation was found. At $\mathrm{Ta}=1.5\times10^6$, the simulation showed a very slow but clear exponential decaying periodic vacillation but this eventually reached a steadily traveling wave with a constant amplitude (steady wave, 3S). At the next value of Taylor number investigated, $\mathrm{Ta}=2.0\times10^6$, the flow showed very weak but persistent irregular fluctuations. The fluctuations were associated with small-scale fluctuations of the increasingly narrow jets visible in Fig. 3. At the first observation of time dependence at $\mathrm{Ta}=2\times10^6$, the fluctuations are so weak that they are not visible in the power spectrum of the cosine component of the wave. The drift of the strong wave pattern dominates the spectrum shown by the upper spectral curve in Fig. 4(a). Only when the wave propagation is eliminated by calculating the power spectrum of the wave amplitude, shown in the lower curve in Fig. 4(a), can the fluctuations clearly be seen. As Fig. 4(a) demonstrates, the spectrum of those fluctuations has a very broad signature in frequency, even at this weak amplitude. At the higher Taylor number, $\mathrm{Ta}=3.25\times10^6$, the fluctuations are clearly visible in both the amplitude power spectrum and that of the cosine component in Fig. 4(b).

Figure 5 shows two time-averaged azimuthal wavenumber spectra for (a) a steady wave at $\mathrm{Ta}=1.5\times10^6$ and (b) a time-dependent case at $\mathrm{Ta}=4\times10^6$. While the earlier discussed transition to time dependence on the $m=2$ branch, from 2S to 2AV, was characterized by a fundamental change in the time-averaged spectrum,[14] the azimuthal mode spectra for all wave-3 flows are qualitatively similar. The only substantial change coinciding with the transition to time-dependent behavior is the increase in amplitude of the "floor" of wave modes which are not higher harmonics of the dominant $m=3$ from around 10^{-4} dimensionless units to around 10^{-3}. Increasing the Taylor number beyond $\mathrm{Ta}=2\times10^6$ up to $\mathrm{Ta}=5\times10^6$ has no further effect on the time-averaged spatial spectrum. We recall that for the steady wave flow dominated by baroclinic instability at lower rotation rates, characterized by $\mathrm{Fr}_a<1$, the contribution of nonharmonic modes in the azimuthal wavenumber spectra is essentially zero (see, for example, Fig. 4 in Randriamampianina *et al.*[14]). The increase in the level of nonharmonic modes obtained for this centrifugally dominated steady wave flow $(3,1+3)S$ at $\mathrm{Ta}=1.5\times10^6$ is inferred from the presence of the higher radial mode, as indicated in Fig. 2.

C. Radial and vertical structure of the steady waves

At relatively low values of the Taylor number ($\mathrm{Ta}\lesssim4\times10^5$), the three-dimensional spatial structure was that of a typical baroclinic wave, qualitatively very similar to that of the steady $m=2$ wave except for the different azimuthal wave numbers. The azimuth-height maps at midradius in Fig. 6 show a pressure field which tilts westward with height and the temperature and vertical velocity fields which tilt eastward in such a way that the strongest upwelling is located around the strongest temperature gradient and strongest pres-

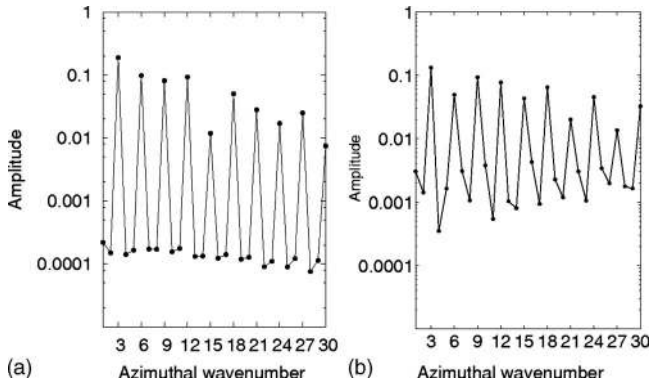

FIG. 5. Azimuthal wavenumber spectra, showing the time-averaged amplitudes of the different wave modes for Taylor numbers, (a) 1.5×10^6 and (b) 4.0×10^6.

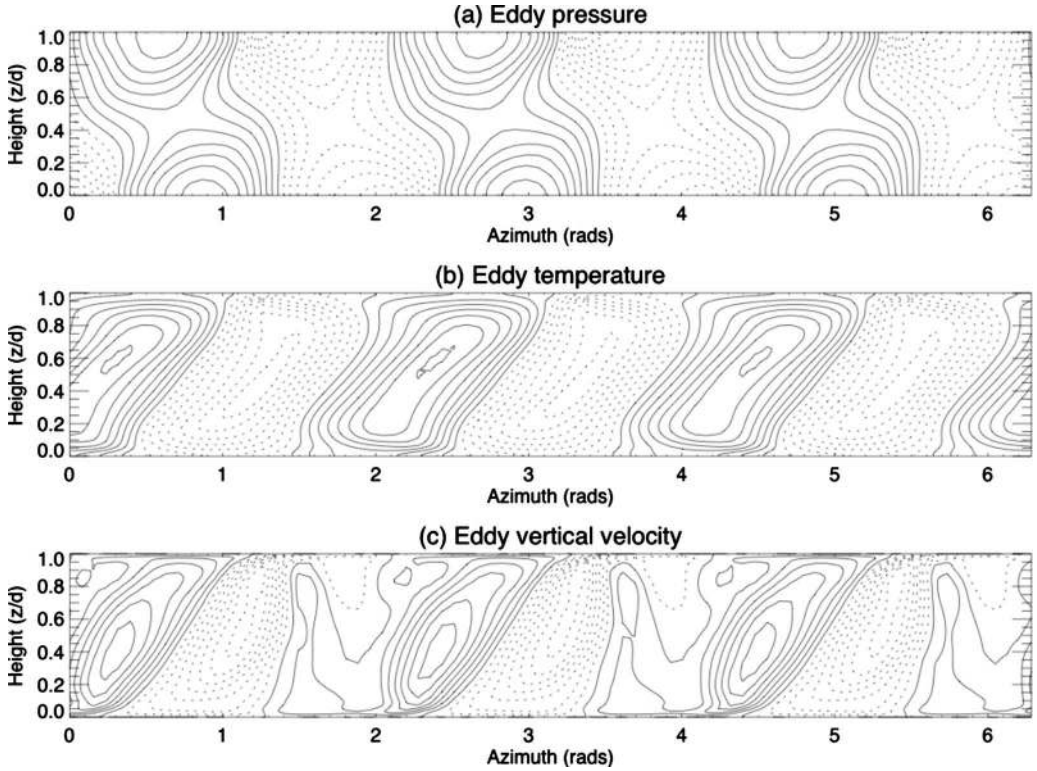

FIG. 6. Azimuth-height maps of eddy fields (with azimuthal flow removed) of a wave-3 simulation at relatively low Taylor number $\mathrm{Ta}=0.235\times10^6$. (a) Pressure (contour interval=0.25 dimensionless units), (b) temperature T (contour interval=0.05, normalized to an imposed temperature difference of ±1.0), and (c) vertical velocity (contour interval=0.5 dimensionless units).

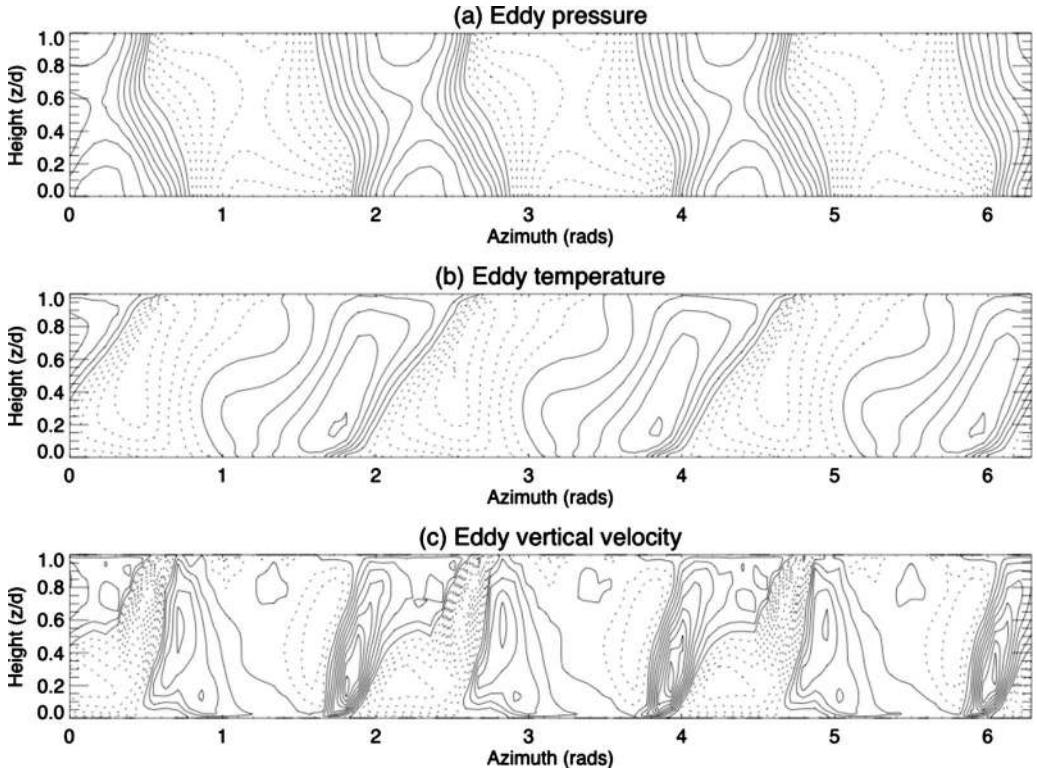

FIG. 7. Azimuth-height maps of eddy fields (with azimuthal flow removed) of a wave-3 simulation at intermediate Taylor number $\mathrm{Ta}=5\times10^5$. (a) Pressure (contour interval=0.25 dimensionless units), (b) temperature T (contour interval=0.05, normalized to an imposed temperature difference of ±1.0), and (c) vertical velocity (contour interval=0.5 dimensionless units).

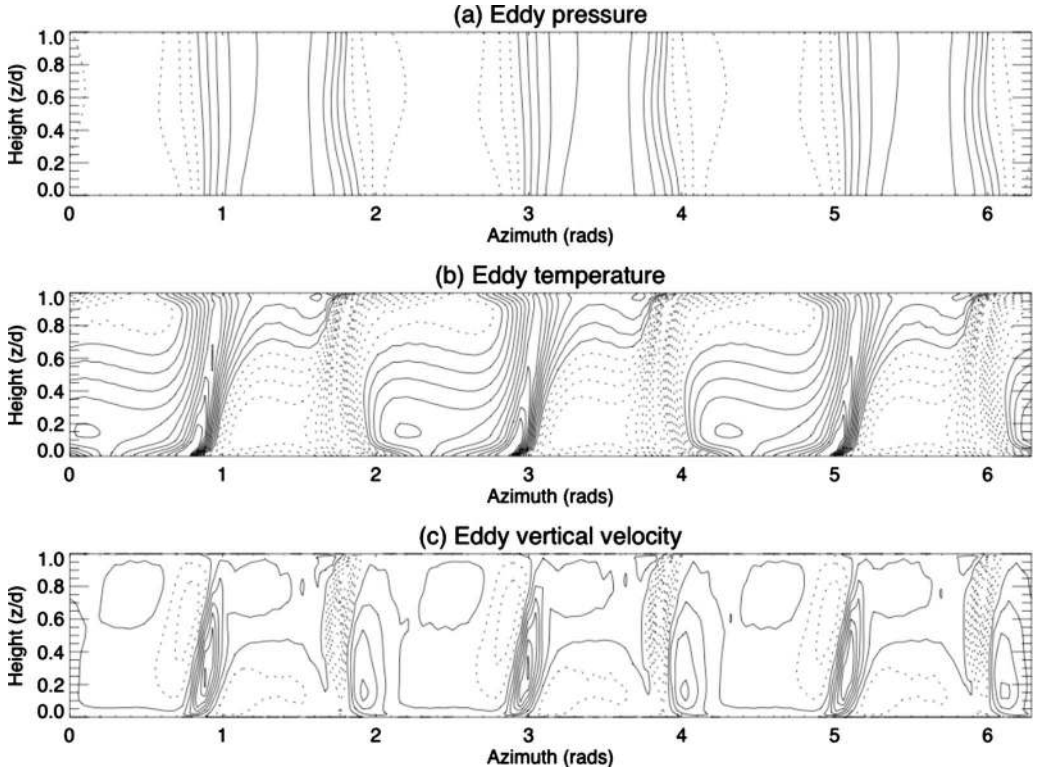

FIG. 8. Azimuth-height maps of eddy fields (with azimuthal flow removed) in a simulation of the wave-3 flow at $\mathrm{Ta}=1.5\times10^6$. (a) Pressure (contour interval=0.25 dimensionless units), (b) temperature T (contour interval=0.05, normalized to an imposed temperature difference of ±1.0), and (c) vertical velocity (contour interval=0.5 dimensionless units).

sure gradient near the ground. In corresponding azimuth-height maps at higher Ta and Fr_a (Figs. 7; $\mathrm{Ta}=5\times10^5$, and Fig. 8; $\mathrm{Ta}=1.5\times10^6$), both the pressure distribution and the temperature show first only a slight reduction in their tilt, but the vertical velocities concentrate into narrower plumes which are also noticeably less tilted than the temperature and pressure fields. Eventually, the decrease of the tilt results in a virtually vertical, barotropic structure, as illustrated, e.g., in Fig. 8 for $\mathrm{Ta}=1.5\times10^6$. The pressure field [Fig. 8(a)] clearly shows very little phase tilt with height while the temperature field exhibits highly concentrated plumes of hot and cold air, which have very little slope with height, interspersed with broad regions with relatively very weak horizontal thermal gradients. The thermal plumes are azimuthally aligned with the regions of strong azimuthal pressure gradient, consistent with optimizing the correlation between radial (geostrophic) velocity and temperature perturbations. Similarly, the regions of strong upward vertical velocity [Fig. 8(c)] are also concentrated close to the strongest positive temperature anomalies, and *vice versa*, consistent with an optimization of $\overline{w'T'}$ (where w' and T' represent departures in vertical velocity and temperature from their azimuthally averaged values). Regions of strong downward motion (necessary to satisfy mass conservation) are concentrated in plumes or jets adjacent to the strong upwelling jets, forming "cross-frontal" circulations which show some similarities with those inferred for atmospheric frontal regions in developing cyclones.[38] The overall impression is that the flow in this region of parameter space is strongly nonlinear and much modified from the simple, linearly unstable Eady solution found in Fig. 6 and the corresponding state for $m=2$ flows at much lower Taylor number.[14]

The azimuthally averaged fields at low values of the Taylor number, shown in the top row in Fig. 9, again are typical of a classical baroclinic wave with steeply inclined isotherms in (i.a), the vertical shear of the thermal wind in the zonal velocity (i.b), and the corresponding symmetric circulation in the meridional stream function in Fig. 9(i.c). At $\mathrm{Ta}=0.3\times10^6$—which corresponds to $\mathrm{Fr}_b=1.25$, $\mathrm{Fr}_a=0.72$, and $\mathrm{Fr}_c=1$—the isotherms in the middle row of Fig. 9(ii) show a weak flattening in the fluid interior in the azimuthally averaged temperature field. Together with this, the zonal jets in Fig. 9(ii.b) are shifted sideways, the upper layer toward the outer radius and the lower toward the inner radius, leading to a mixed baroclinic-barotropic velocity shear. Increasing the Taylor number to $\mathrm{Ta}=0.4\times10^6$ or $\mathrm{Fr}_a=0.9$ virtually completes the transition with almost horizontal isotherms at midheight. Beyond this, the features qualitatively stay the same and only intensify. The isotherms in Fig. 9(iii.a) for $\mathrm{Ta}=0.5\times10^6$ even have a slight inversion against the imposed temperature difference. Furthermore, the meridional stream function, which showed two overturning cells at the lower Taylor number in Fig. 9(i.c) has developed a clear third counter-rotating cell in the center of the annulus in Fig. 9(iii.c).

This transition can be summarized in Fig. 10 by the magnitude of the local temperature gradient at midradius and midheight. The figure shows the azimuthally averaged values (as circles) and their extreme values (as triangles) against the local Froude number Fr_c at the midchannel radius $(a+b)/2$.

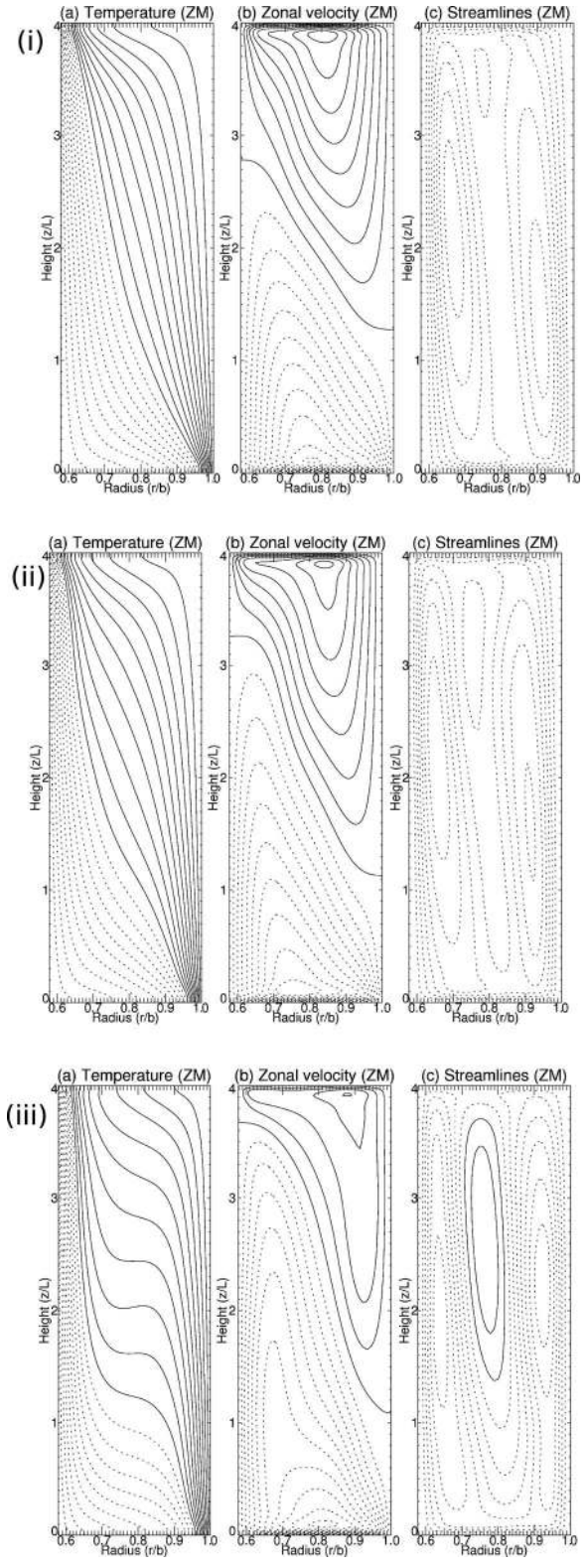

FIG. 9. Azimuthally averaged fields for wave-3 simulations at three values of the Taylor number, top row (i). $\mathrm{Ta}=0.235\times10^6$, the same case as in Fig. 6, middle row (ii). $\mathrm{Ta}=0.3\times10^6$, and bottom row (iii). $\mathrm{Ta}=0.5\times10^6$. (a) Temperature (contour interval=0.1, normalized to an imposed temperature difference of ±1.0), (b) zonal velocity v (contour interval=0.25 dimensionless units), and (c) meridional stream function (contour interval=0.01 dimensionless units).

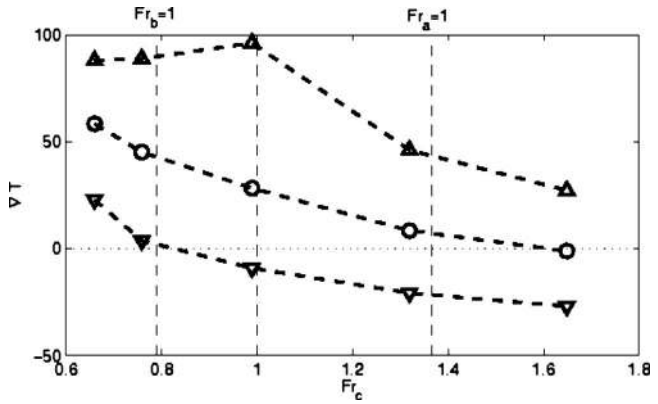

FIG. 10. Magnitude of the temperature gradient at midradius and midheight against the local Froude number $\mathrm{Fr}_c=\Omega^2(a+b)/(2g)$. The Froude numbers cover the range of Taylor number from 0.2×10^6 to 0.5×10^6.

The vertical dashed lines at $\mathrm{Fr}_c=0.79$ and at $\mathrm{Fr}_c=1.36$ indicate where the local Froude numbers at the outer and inner radii are equal to $\mathrm{Fr}_b=1$ and $\mathrm{Fr}_a=1$, respectively. At low Froude numbers, or $\mathrm{Fr}_b\lesssim1$, the temperature gradient is always positive while, at higher Froude numbers, $\mathrm{Fr}_a\gtrsim1$, the azimuthally averaged temperature gradient is around zero. This reduction occurs in two stages. First, the range of gradient is substantially extended, especially to smaller values of the gradient. At around $\mathrm{Fr}_c\approx1$, the minimum gradient is actually in the opposite direction to the imposed temperature gradient due to a tightening and tilting of the wave lobes or plumes, and perhaps also due to convective overshoot. In the second stage, the range reduces again, so that the gradient becomes fairly symmetric about a zero gradient.

D. Time-dependent flow

A snapshot of the fields at $\mathrm{Ta}=4\times10^6$ in any of the sections in Fig. 11 shows fields qualitatively very similar to those of the steady waves at $\mathrm{Ta}=1.5\times10^6$ and even as low as $\mathrm{Ta}=0.5\times10^6$, the columnar form of the flow patterns with extremely concentrated gradients is even more pronounced. The shape of the plumes or jets is clearly illustrated by temperature profiles around the annulus at three radial positions, shown in Fig. 12(a) (all at midheight). For a clearer visualization, the three profiles are plotted on the same temperature axis, with each shifted by 0.5 temperature units. The three warm jets form near the outer wall (upper dotted line) as relatively broad features but then become highly concentrated in the center (middle solid line) before spreading out again as they approach (and interact with) the inner boundary (lower dot-dashed line). The three plumes appear virtually identical, bar some very small variations near the temperature extrema at the outer and inner locations. The return flow, radially outward in the cold plumes, shows much less spreading, especially in the inner part of the annulus. The same features are reproduced in the time series of the temperature at a single point along these cross sections. The time series in Fig. 12(b) cover one phase period, that is, the time over which one jet has azimuthally moved by one wavelength. The additional features in the time series are fluctuations at a time scale of 20–30 nondimensional time units.

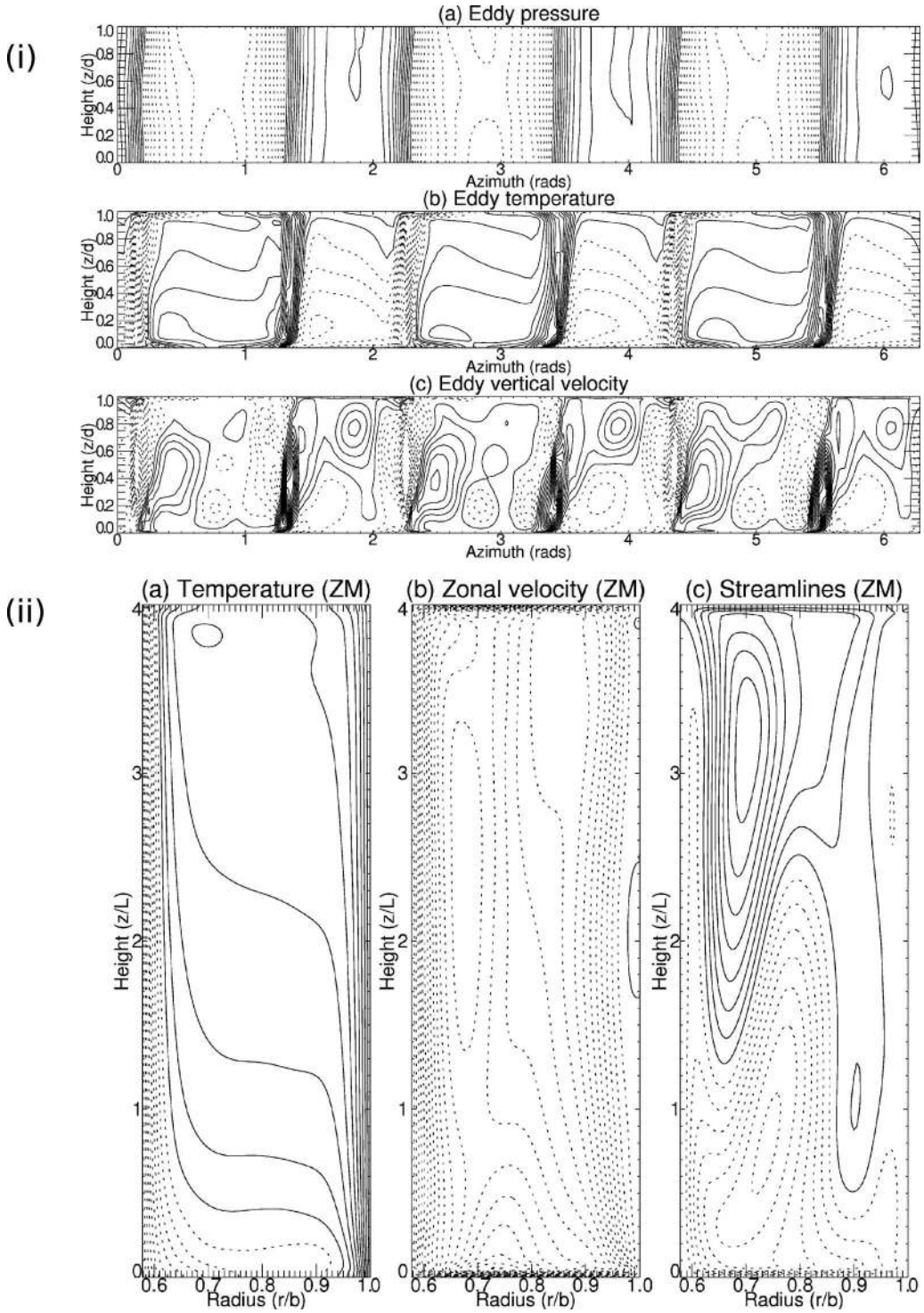

FIG. 11. Instantaneous fields from a simulation of the vacillating wave-3 simulation at $\mathrm{Ta}=4\times10^6$; (i) azimuth-height sections of "eddy" fields at midradius. (a) pressure (contour interval=0.25 dimensionless units), (b) temperature (contour interval=0.05, normalized to an imposed temperature difference of ±1.0), and (c) vertical velocity (contour interval=0.5 dimensionless units); (ii) zonally averaged fields. (a) temperature (contour interval=0.1), (b) zonal velocity (contour interval 0.25), and (c) the meridional stream function (contour interval=0.01).

While they are weak but clearly visible near the boundaries, they are virtually invisible in the center. These fluctuations become clearly visible in the time series of the azimuthal wave amplitudes in Figs. 13(a) and 13(b) at midradius and three quarters of the gap, respectively.

The first observation is that the much narrower structure of the jets in the center is reflected by the relative strength of the average amplitudes, namely, that $m=3$ is only marginally stronger than its harmonics, especially the third harmonic [as also shown earlier in Fig. 5(b)]. Another feature of these two sets of time series is the relative phase of the amplitude variations; at the center, modes $m=3$ and 9 are virtually oscillating in phase but modes $m=6$ and 12 in antiphase to $m=3$. Nearer the outer wall, however, modes $m=3$, 9, and 12

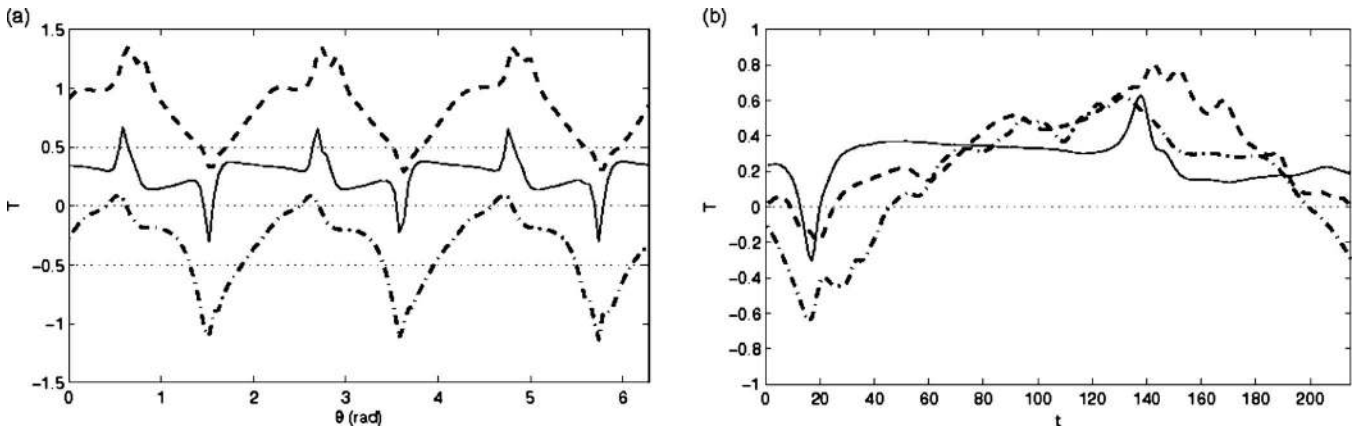

FIG. 12. Temperature data from the vacillating wave-3 simulation at $\mathrm{Ta}=4\times10^6$ at midheight; (a) azimuthal profiles at a quarter of the gap (dot-dashed line), midradius (solid line), and three quarters of the gap (dashed line) from the inner cylinder. The temperature axis refers to the temperature at midradius, while the other two lines are shifted by ±0.5 where the dotted lines indicate their respective $T=0$ axis. (b) Time series of the temperature at a fixed azimuthal point ($\theta=0$) for the same three radial positions over one phase period.

approximately oscillate in phase and only $m=6$ is in antiphase to them. By comparing the oscillations between the two radial positions, it appears that it is the mode $m=12$ which oscillates in phase across the gap. This spatio-temporal phase shift of the mode amplitudes is mirrored by a radial shift of the spatial phase of the modes. Figure 13(c) shows the time series of the difference between the spatial phase of the waves $m=3$, 6, 9, and 12 at midradius and the phase at three quarters of the gap width. This shows that the wave-3 shows a significant but fairly constant phase shift

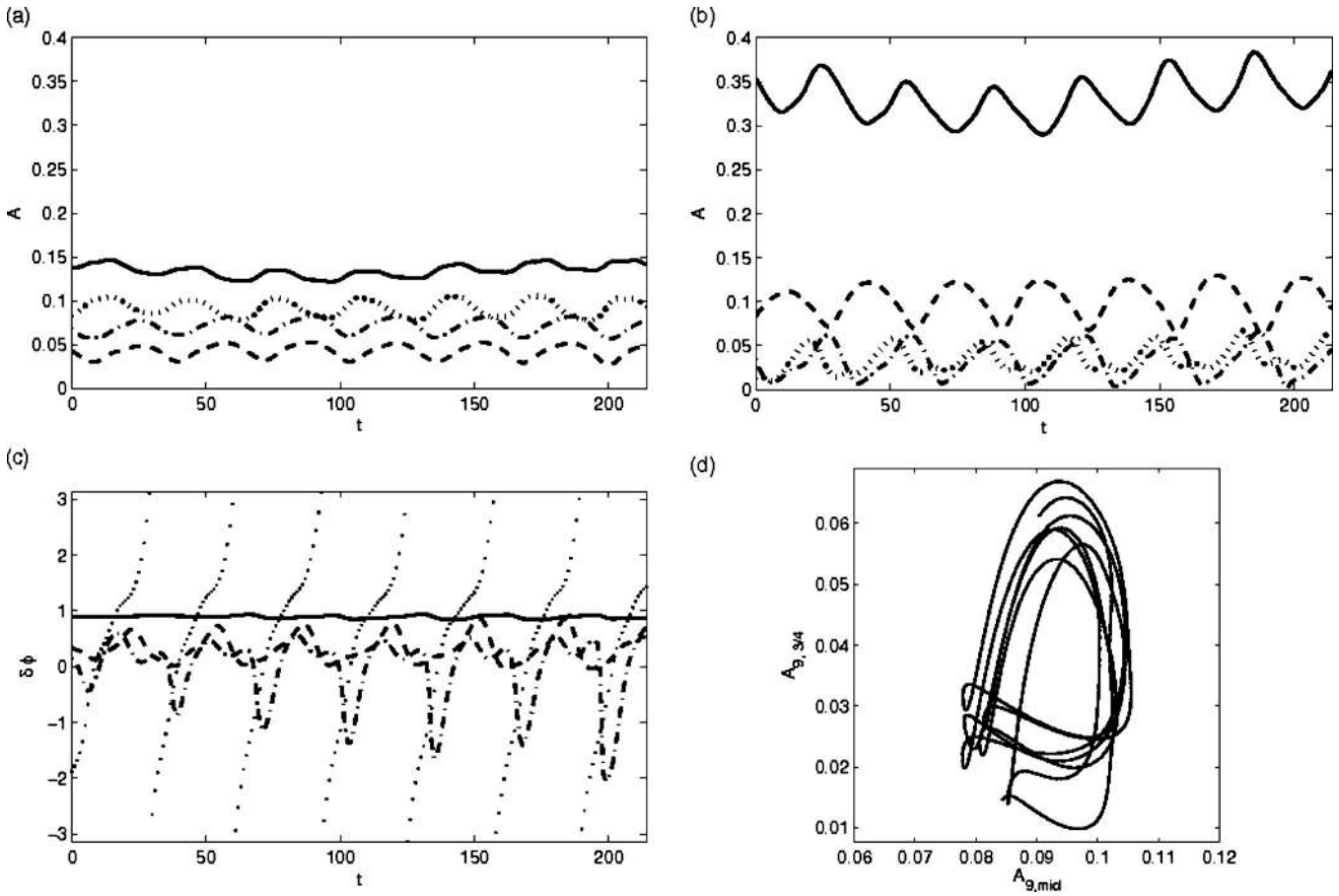

FIG. 13. Azimuthal Fourier mode data from the vacillating wave-3 simulation at $\mathrm{Ta}=4\times10^6$ at midheight for the dominant azimuthal wave mode and its first three higher harmonics in (a) to (c). $m=3$ (solid lines) $m=6$ (dashed lines) $m=9$ (dotted lines), and $m=12$ (dot-dashed lines). (a) Time series of the amplitude at midradius; (b) as for (a) but at three quarters of the gap from the inner cylinder. (c) Time series of the phase difference between an azimuthal mode at midradius and the same mode at three quarters of the gap. (d) Phase portrait using the time series of the amplitude of mode $m=9$ at three quarters of the gap against that at midradius.

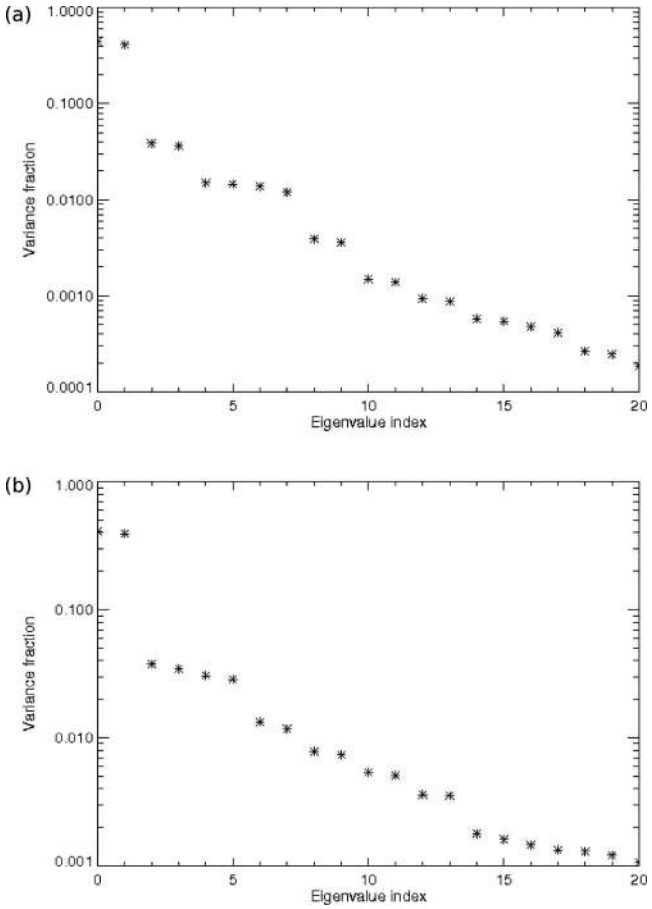

FIG. 14. Eigenvalue spectra from the EOF analysis of time series of horizontal sections at midheight from simulations of a wave-3 flow. (a) Taylor number $Ta=1.5\times10^6$ and (b) Taylor number $Ta=4\times10^6$. Note the change of vertical scale between (a) and (b).

across the gap. The wave modes $m=6$ and 12 appear to oscillate around a mean value, while the mode $m=9$ near the boundary appears to lock to that at the center for part of the oscillation cycle but then loses synchronization, as shown by a rapid divergence of the phase difference from a value of around $\pi/2$ until it begins to lock in again just after a zero phase difference. The modulation of the oscillation cycles is illustrated in the phase portrait in Fig. 13(d). While the length of this timeseries is fairly limited, it is clear that the oscillation is not simply periodic but modulated with a longer period.

1. Horizontal EOF analysis

To identify what might be the essential dynamical difference between the steady flow at $Ta=1.5\times10^6$ and the vacillation at $Ta=4.0\times10^6$, an EOF analysis was performed on time series of horizontal temperature fields at midheight for both cases. Figure 14 shows the spectra of the eigenvalues for the two cases, both of which are dominated by a pair of eigenvalues corresponding to the dominant traveling wave-3 pattern. In the case of the steady wave, the first two modes contribute 85.3% to the variance of the full field which slightly drops to 81.7%. In both cases, the second pair contributes a little over 7% (steady case: 7.5%, vacillating case: 7.2%). A small but marked difference can finally be seen in the third pair, which only contributes 3% in the steady case but twice as much in the vacillating case (5.9%). The tail of the spectrum is again very similar for the two cases, except that it decays more rapidly at high order for the steady flow [Fig. 14(a)].

Figure 15 illustrates temperature EOFs at midheight at $Ta=1.5\times10^6$. The first six EOFs represent more than 95%

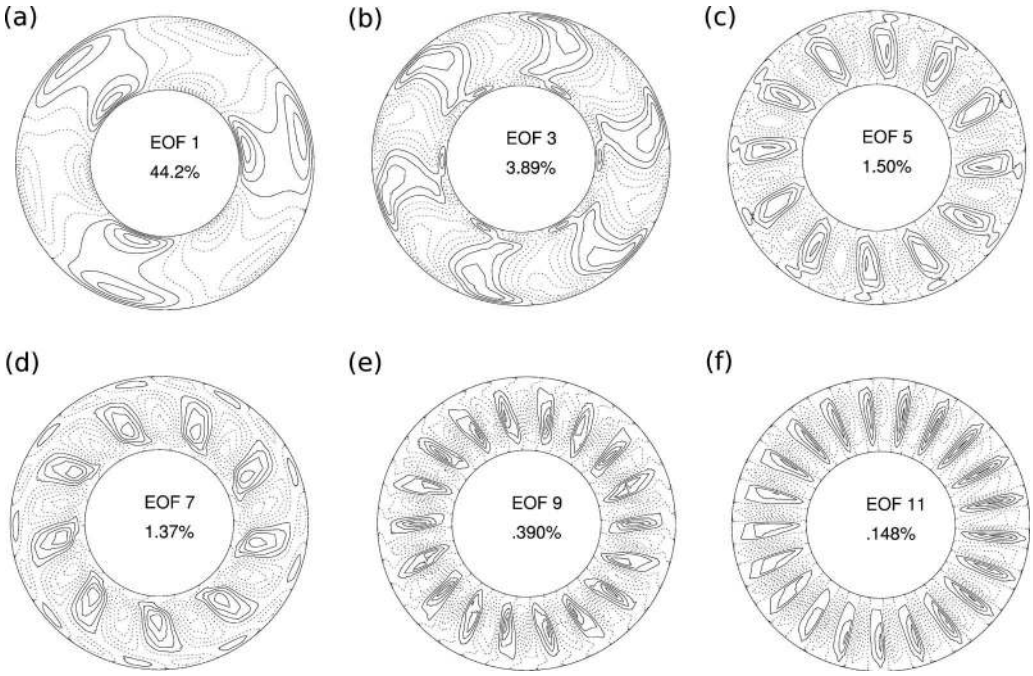

FIG. 15. Maps of the odd EOFs from the first six pairs of EOFs of temperature at midheight from the wave-3 simulation in air at $Ta=1.5\times10^6$. EOFs are shown in order of decreasing contribution to the total temperature variance at this level. The even EOFs are spatially very similar to their preceding odd EOFs except for a phase shift of a quarter phase of the wave pattern.

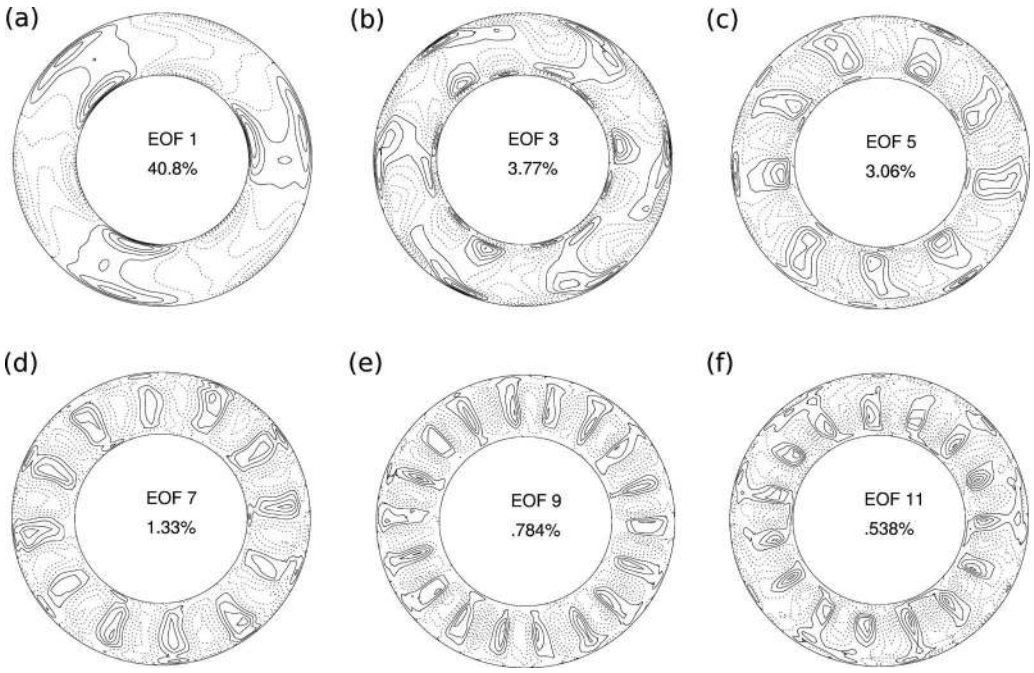

FIG. 16. Maps of the odd EOFs of the first six pair EOFs of temperature at midheight from the vacillating wave-3 simulation in air at $\mathrm{Ta}=4.0\times10^6$. EOFs are shown in order of decreasing contribution to the total temperature variance at this level.

of the temperature variance at this level. They appear as three *conjugate pairs*, in which the two members of each pair have similar spatial structures but one is azimuthally displaced with respect to the other by a quarter wavelength of the dominant azimuthal Fourier mode. In this respect, the conjugate pair of EOFs resemble a sine-cosine pair in a Fourier decomposition. Figure 15(a) represents a pattern dominated by $m=3$, with all radii in phase azimuthally, but with two maxima in amplitude with radius close to each of the inner and outer boundaries. The temperature amplitude has a local minimum near midradius. Figure 15(b) is dominated by the first azimuthal harmonic, $m=6$, but with a complicated structure in radius. In particular, a π azimuthal phase reversal with radius occurs near the inner cylinder, beyond which the azimuthal phase first decreases then increases again toward the outer boundary. The higher order EOFs in Figs. 15(c) and 15(d) generally have a much simpler radial structure, with a simple maximum in amplitude near midradius and only weak phase tilts with radius. They again appear in conjugate pairs and represent other azimuthal harmonics of $m=3$, e.g., $m=12$ [(c)], $m=9$ [(d)], $m=18$ [(e)], and $m=21$ [(f)].

At $\mathrm{Ta}=4.0\times10^6$, the spatial structure of the temperature EOFs at this level is actually quite similar to that found at 1.5×10^6. Figures 16(a)–16(f) show the first six pairs of EOFs for this case, which together account for a little over 98% of the temperature variance, compared to over 99% at 1.5×10^6. In this case, however, the first three pairs of EOFs represent 93.2% of the variance, indicating a slightly broader spread into the higher order patterns. The first two EOFs [Fig. 16(a)] have a relatively similar structure to the first two EOFs in Fig. 15, except that the radial structure seems somewhat more concentrated toward the side boundaries, with only weak amplitude distributed throughout most of the interior radii. EOFs 3 and 4, Fig. 16(b), again, show a pattern dominated by $m=6$, but with even more contorted phase shifts with radius. The overall impression is of a pattern represented by $m=6$ in azimuth and $l=4$ in radius (where l is a nondimensional radial wavenumber). Subsequent EOFs again show patterns with a reasonably simple $l=1$ radial structure [except for (c), which also shows evidence for $l=4$ dependence on r in EOFs 3 and 4], and increasing azimuthal harmonics of $m=3$. The main difference from $\mathrm{Ta}=1.5\times10^6$ is that the $m=9$ and $m=12$ groups are interchanged in order, suggesting a change in relative amplitude of these two pairs of modes as Ta increases (see also Fig. 5).

The complex phase variations with radius in EOFs 3 and 4 demonstrate the growth of higher radial modes as previously indicated in Fig. 2, though the patterns in (c) and (d) of Figs. 15 and 16 would seem to suggest such anticorrelations ought to be strongest for $m=6$ rather than the dominant $m=3$.

2. Principal components and the onset of SV

The detailed behavior of the time evolution of the flow and, in particular, of the signatures of the onset of structural vacillation, is to some extent obscured in the principal components (PCs) by the drift of the overall pattern as illustrated by the first six PCs of the simulation at $\mathrm{Ta}=4.0\times10^6$ in Fig. 17. These patterns were obtained by projecting each EOF onto the time sequence of the original temperature fields. Much as expected, this shows a set of basically sinusoidal oscillations associated with the uniform drift of each component at a roughly constant angular velocity around the annulus. Thus, Figs. 17(a) and 17(b) show a single cycle corresponding to a drift of the $m=3$ pattern by one wavelength in this time interval, whereas (c) and (d) show two cycles cor-

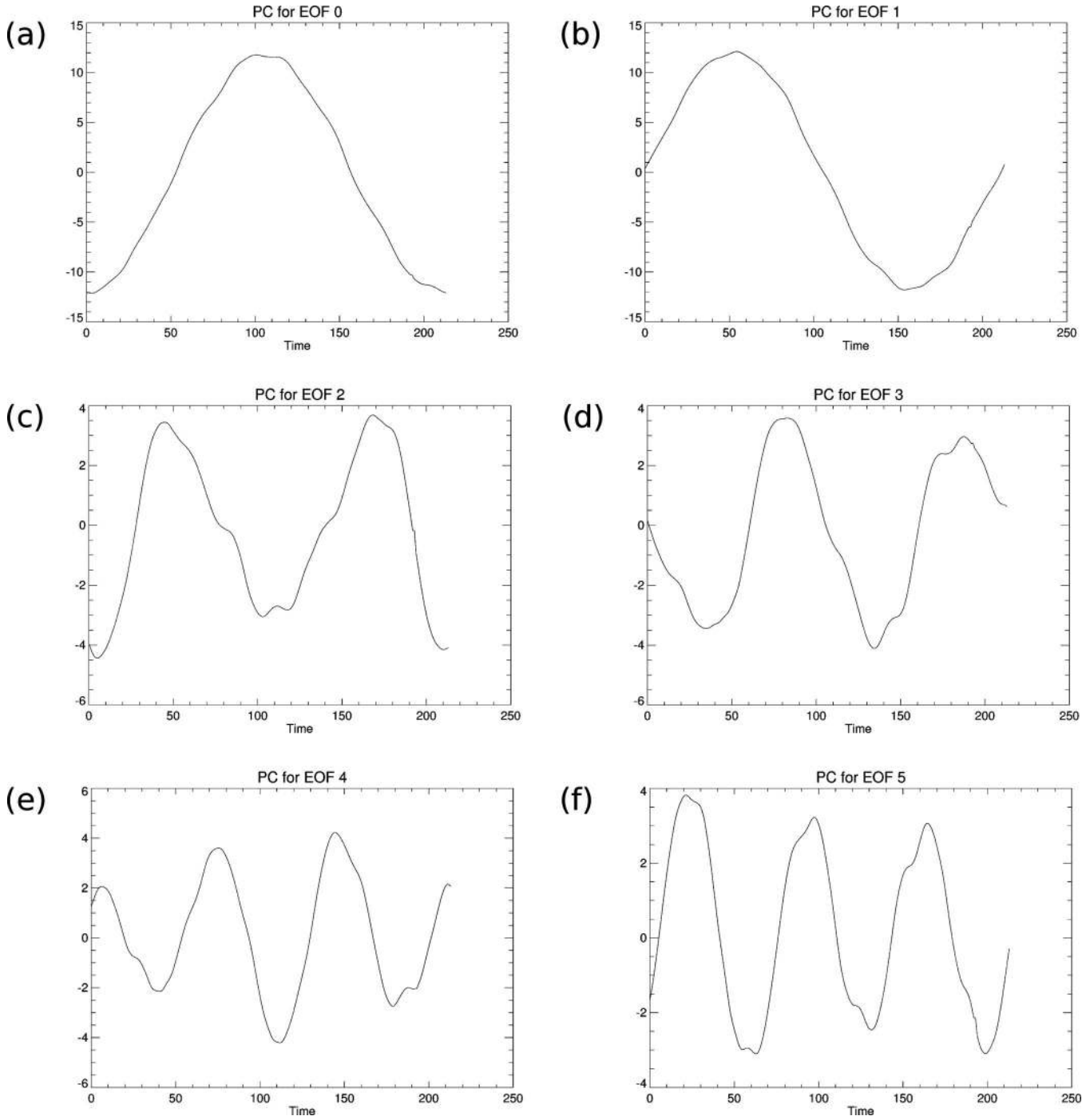

FIG. 17. Principal components of the first six EOFs of temperature at midheight from the vacillating wave-3 simulation in air at Ta=4.0×10^6.

responding to $m=6$, (e) and (f) show three cycles for $m=9$, and so on. Especially, the pair of PCs 1 and 2 appear almost like $a-\cos$ and sin of a traveling steady wave with a phase drift period of about 220 time units. Nevertheless, some fluctuations are visible superimposed on the pattern drift. The additional oscillations are most prominent for the third and fourth EOFs, corresponding to modulations of the amplitude of the complex $(m,l)=(6,4)$ mode and in PCs 5 and 6, which show a slow modulation of that oscillation representing a slower modulation of $(m,l)=(9,4)$.

The modulations of the amplitude appear more clearly by considering the combined amplitude of a pair of PCs, by taking the square root of the sum of the squares of two PCs belonging to a conjugate pair of EOFs. This amplitude is shown for the first four wave amplitudes in Fig. 18. The amplitudes of the higher pairs of PCs is substantially smaller than that of the first pair. However, they show an intricate interplay between those higher pairs, while the first pair, associated with the azimuthal mode, $m=3$, is relatively steady.

3. Lyapunov exponents

The results so far have indicated the onset of some rapid, irregular time dependence in the flow at a well defined value

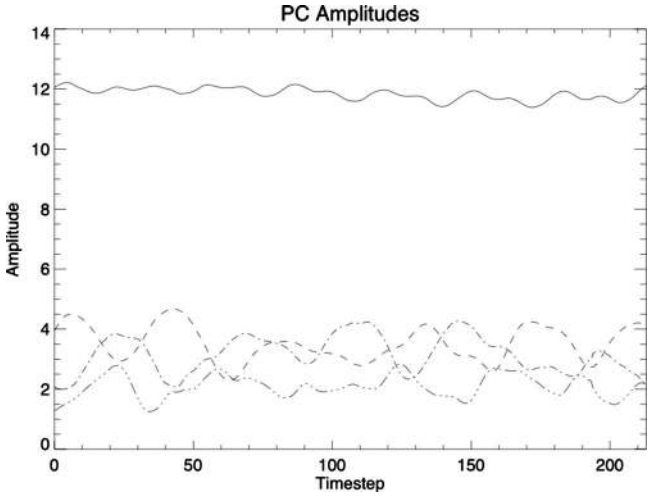

FIG. 18. Amplitudes of the first four pairs of principal components of temperature at mid-height from the vacillating wave-3 simulation in air at Ta $=4.0\times10^6$. Amplitudes represent $\sqrt{a_n^2(t)+a_{n+1}^2(t)}$, where $a_n(t)$ is the time-dependent principal component of EOF n. The solid line shows the amplitude of EOF pair 1+2, the dashed line EOFs 3+4, dot-dashed line EOFs 5+6, and double dot-dashed line EOFs 7+8.

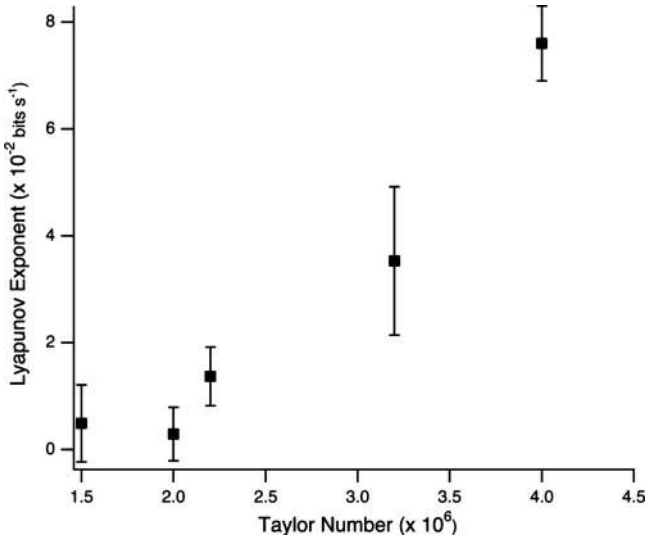

FIG. 19. Variation of the largest non-negative Lyapunov exponent as a function of Taylor number, derived from temperature time series at mid-height and midradius.

of Ta. However, it is of interest and importance to establish whether the onset of this new mode of time dependence results in chaotic or regular oscillations. In this regard, the most fundamental measure of chaotic behavior, namely, the sensitivity of the trajectory to initial conditions, is the largest non-negative Lyapunov exponent. In the present work, we have computed estimates of the largest Lyapunov exponent by using a variant of the algorithm by Wolf *et al.*[39] applied to a time series of temperature at a fixed point in the flow (at midheight and midradius), densely sampled in time over several drift periods. In the present application, however, we refine the delay embedding by using singular systems decomposition, essentially as used by Read *et al.*[8] The growth of perturbations was then computed by using segments of the time series which began within $10^{-3}\leqslant\delta\leqslant5\times10^{-2}$ of each other and evolved for a time interval of 20 time units. The computation was then repeated for each of embedding dimensions k from 3 to 9. In all cases, the Lyapunov exponent λ had converged by $k=5-7$, indicating relatively low-dimensional behavior.

The results for a range of different values of Ta are shown in Fig. 19. Error bars are shown which indicate the standard error on the mean of the set of computations of λ for each set. From this, it is clear that for $\mathrm{Ta}\leqslant2\times10^6$ the Lyapunov exponent is indistinguishable from zero, indicating a quasiperiodic or steady flow. The result of $\lambda\approx0$ at $\mathrm{Ta}=2.0\times10^6$ is very robust against changing the parameters such as minimum and maximum distances for following the trajectory. This appears at odds with the observation from a time series of the wave amplitude and from its power spectrum. However, as was pointed out, the magnitude of those fluctuations was so small that it was not visible in the full temperature data. It appears therefore that such small fluctuations would either not affect the large-scale flow and its predictability or that its effect on trajectory spreading was slower than the integration time for that simulation. For Ta $=2.2\times10^6$, however, λ is significantly positive and continues to monotonically increase with increasing Ta. This corresponds to a transition to weak SV, indicating that the vacillation is probably immediately chaotic and that the Lyapunov exponent increases in line with the magnitude of the fluctuations with a critical Taylor number very close to $\mathrm{Ta}=2.0\times10^6$. The nature of this transition leading to SV is not obviously apparent.

V. DISCUSSION

As is clear in the results presented above, at the high values of Ta considered here, an entirely different transition sequence was observed from the 3S flow compared to that of the $m=2$ flows presented by Randriamampianina *et al.*[14] A fundamental difference lies in the structure of the flow fields in components other than the azimuthal wave number. Throughout the $m=2$ wave regimes discussed by Randriamampianina *et al.*,[14] the radial and vertical structures remained largely unchanged. The radial spectrum was dominated by the first mode (with a single antinode across the domain) and with a radial-vertical structure typical of fully developed baroclinic waves, as described previously by Hide and Mason,[4] with strongly inclined isotherms, narrow Ekman layers at the top and bottom, and wider Stewartson layers at the side boundaries. This was completed by an eastward tilt with height of the temperature field in height-azimuth sections and a corresponding westward tilt of the pressure field. After the transition to the $m=3$ flows, this structure of a typical fully developed baroclinic wave was also observed but, on increase of the Taylor number or Froude number, the steady wave underwent a structural change from that of the baroclinic wave to what appeared to be a set of steady columnar convection cells with an essentially barotropic structure. That change occurred in a transition which was gradual but largely restricted to a range of parameters during which the local Froude number crossed unity at some radius within the fluid, $\mathrm{Fr}_a<1<\mathrm{Fr}_b$. Within that parameter range, the cur-

vature of the isopotential surfaces increased under the combined action of gravity and centrifugal acceleration such that the isopotential surfaces were inclined less than 45° everywhere below that range but more than 45° everywhere above that range. The direction of the azimuthally averaged local temperature gradient at midheight and midradius responded to that change in the local effective gravity by gradually changing from nearly horizontal to essentially vertical relative to the local (centrifugally modified) geopotential surface. It seems that the observed changes reflect a switch over from baroclinic instability to the rotational equivalent of Rayleigh–Bénard convection under radial centrifugal buoyancy within that clearly defined parameter range defined by the local Froude number.

A decomposition into global modes by EOF analysis of time series of horizontal sections suggests that a very large proportion of the variance of the large-scale structure can be described by a single pair of EOFs, i.e., that they behave as a single mode in temperature with a well defined azimuthal wave number $m=3$ and a complex but fixed radial structure, which would consist of several radial modes in a spectral description. Upon crossing the $\mathrm{Fr}_a=1$ boundary, the radial structure of the dominant azimuthal wavenumber and its first harmonic underwent a rapid change from a simple unimodal form with a single antinode to a more complex, multimodal structure with spiral phase shifts across the annular gap. The latter structure is reminiscent of some of the high-order traveling wave modes found in rotating annulus convection with centrifugal buoyancy by Pino *et al.*,[23] who used numerical continuation techniques to follow steady, azimuthally traveling wave solutions to the Navier–Stokes equations from (mostly supercritical) Hopf bifurcations. Such radially complex steady wave solutions were found to be stable in air for values of the centrifugal Rayleigh number ($\simeq \mathrm{Ra}\cdot\mathrm{Fr}_c$ in our notation) in excess of 1.6×10^5. Such values are approximately consistent with our simulations, for which[14] $\mathrm{Ra}=4.733\times10^4$ and $1<\mathrm{Fr}_c\leqslant10$.

Rather than undergoing a classifiable bifurcation sequence from steady to chaotic behavior, however, as was found in the set of bifurcations to a chaotic 2MAV flow at the lower Taylor numbers and to steady traveling waves in the centrifugal buoyancy regime by Pini *et al.*,[23] the convection columns appeared to develop weak, but immediately irregular, time-dependent fluctuations at a critical Taylor number of $\mathrm{Ta}=2.0\times10^6$ or Froude number $\mathrm{Fr}_a=4.8$. On further increase of the Taylor number, those fluctuations became gradually stronger, and the largest Lyapunov exponent increased in line. It is possible that a supercritical bifurcation to a quasiperiodic vacillation does occur in the range $\mathrm{Ta}=(1.5-2)\times10^6$. If that was the case, it would have to be pointed out that such a vacillation would be too weak to be distinguishable from experimental noise in all annulus experiments carried out so far. By $\mathrm{Ta}\geqslant3.25\times10^6$, however, the fluctuations are sufficiently strong to be observable in most experiments.

The behavior found there is substantially different from that of regular or chaotic amplitude vacillations. The vacillation is not described by the variation in the amplitude of the single pair of EOFs describing the dominant mode of the flow (as in amplitude vacillation of baroclinic waves) but by the interchange between higher order EOFs, where the leading pair of EOFs appears to be only weakly involved. As a result, it is the structure of the flow which changes with the oscillations of the higher pairs of EOFs, and the flow could be classified as a SV, 3SV. In the present case, therefore, the simulations demonstrate a case of incipient SV. The time series of wave amplitudes and the phase portraits would seem to suggest that the SV at $\mathrm{Ta}=3.25\times10^6$ is close to being quasiperiodic, but with some persistent noisy irregularities superposed. A sustained noise component has also been previously reported in laboratory experiments in the moderately rotating baroclinic regime by Früh and Read[9] in a flow classified as weak SV. In fact, the time series of the wave amplitudes at different radial positions show some striking similarities to the flow presented by them. On the other hand, there is no evidence in the present runs of the kind of intermittent noisy bursts of SV apparent in the earlier experiments of Read *et al.*[8]

By using air as the working fluid, two distinct features were uncovered and reported here and earlier.[14] The first was the observation, at the lower range of Taylor numbers, of a bifurcation sequence in the reverse direction from that known at high Prandtl number. The second, at larger Taylor numbers, was the transition between baroclinic flows and centrifugal convection, associated with the fact that the rotational Froude number and the Taylor number have the same dependency on the rotation rate. The challenges for the way forward are now to build up a coherent description in terms of the solution structures and transitions as well as their underlying physical processes and their dependence of parameters such as the Prandtl number. Such models and understanding should also be further extended to stronger forms of turbulence.

Some immediate questions have arisen from this work. In what way and how does the Prandtl number organize the bifurcations and turbulent transition for baroclinic waves? What are the physical processes leading to the weakly turbulent fluctuations within the otherwise stable centrifugal convection rolls? Is there a physical reason for their apparent similarity to the flow regime found at moderate rotation rates in baroclinically unstable flows and referred to as SV, and what is their relationship? How does this flow develop as the parameters are extended further toward strong turbulence? Work required to move forward will include systematic laboratory experiments of the system described here, not least to verify and validate the range of numerical simulations presented here. This has already been started as a first step in some experiments in Oxford.[28] This, together with reference to previous reports in various fluids, will help to delineate the dominant physical processes across the available parameter space and to develop coherent bifurcation/transition scenarios for the dynamics for a range of Prandtl number from much less than unity to much larger. DNS can complement this by following the onset of weakly turbulent flow at higher Prandtl numbers, but to extend computational modeling to more strongly turbulent flows at any value of the Prandtl number is still beyond current computational capabilities. Large eddy simulations may provide insight into the route by

which the weak fluctuations become progressively stronger and destroy the large scale structure which, in the weakly turbulent flows shown here, appears largely insensitive to the fluctuations.

ACKNOWLEDGMENTS

We are grateful to the Royal Society for their support of this work by funding the initial collaboration between the French and UK partners in a Joint Project Grant. We are also grateful to the British Council, Égide, and the CNRS for funding the later stages of this collaboration. The CPU time for this work was provided by the CNRS—Institut du Développement et des Ressources en Informatique Scientifique (IDRIS, Orsay, France) on the NEC SX-5.

[1] R. T. Pierrehumbert and K. L. Swanson, "Baroclinic instability," Annu. Rev. Fluid Mech. **27**, 419 (1995).
[2] P. L. Read, M. Collins, W.-G. Früh, S. R. Lewis, and A. F. Lovegrove, "Wave interactions and baroclinic chaos: a paradigm for long timescale variability in planetary atmospheres," Chaos, Solitons Fractals **9**, 231 (1998).
[3] P. L. Read, "Transition to geostrophic turbulence in the laboratory, and as a paradigm in atmospheres and oceans," Surv. Geophys. **22**, 265 (2001).
[4] R. Hide and P. J. Mason, "Sloping convection in a rotating fluid," Adv. Phys. **24**, 47 (1975).
[5] R. L. Pfeffer, G. Buzyna, and R. Kung, "Time-dependent modes of thermally-driven rotating fluids," J. Atmos. Sci. **37**, 2129 (1980).
[6] G. Buzyna, R. L. Pfeffer, and R. Kung, "Transitions to geostrophic turbulence in a rotating, differentially heated annulus of fluid," J. Fluid Mech. **145**, 377 (1984).
[7] P. Hignett, A. A. White, R. D. Carter, W. D. N. Jackson, and R. M. Small, "A comparison of laboratory measurements and numerical simulations of baroclinic wave flows in a rotating cylindrical annulus," Q. J. R. Meteorol. Soc. **111**, 131 (1985).
[8] P. L. Read, M. J. Bell, D. W. Johnson, and R. M. Small, "Quasi-periodic and chaotic flow regimes in a thermally-driven, rotating fluid annulus," J. Fluid Mech. **238**, 599 (1992).
[9] W.-G. Früh and P. L. Read, "Wave interactions and the transition to chaos of baroclinic waves in a thermally driven rotating annulus," Philos. Trans. R. Soc. London, Ser. A **355**, 101 (1997).
[10] F. H. Busse and C. R. Carrigan, "Convection induced by centrifugal buoyancy," J. Fluid Mech. **62**, 579 (1974).
[11] F. H. Busse and A. C. Or, "Convection in a rotating cylindrical annulus: thermal Rossby waves," J. Fluid Mech. **166**, 173 (1986).
[12] A. C. Or and F. H. Busse, "Convection in a rotating cylindrical annulus: Part 2. Transitions to asymmetric and vacillating flow," J. Fluid Mech. **174**, 313 (1987).
[13] M. Schnaubelt and F. H. Busse, "Convection in a rotating cylindrical annulus: Part 3. Vacillating and spatially modulated flows," J. Fluid Mech. **245**, 155 (1992).
[14] A. Randriamampianina, W.-G. Früh, P. Maubert, and P. L. Read, "Direct numerical simulations of bifurcations in an air-filled rotating baroclinic annulus," J. Fluid Mech. **561**, 359 (2006).
[15] J. E. Hart, "A laboratory study of baroclinic chaos on the *f*-plane," Tellus, Ser. A **37A**, 286 (1985).
[16] D. R. Ohlsen and J. E. Hart, "The transition to baroclinic chaos on the β-plane," J. Fluid Mech. **203**, 23 (1989).
[17] H.-Y. Weng and A. Barcilon, "Wave structure and evolution in baroclinic flow regimes," Q. J. R. Meteorol. Soc. **113**, 1271 (1987).
[18] B. J. Hoskins, "Stability of the Rossby-Haurwitz wave," Q. J. R. Meteorol. Soc. **99**, 723 (1973).
[19] A. Gill, "The stability of planetary waves on an infinite beta-plane," Geophys. Fluid Dyn. **6**, 29 (1974).
[20] J. Guckenheimer and G. Buzyna, "Dimension measurements for geostrophic turbulence," Phys. Rev. Lett. **51**, 1438 (1983).
[21] R. Salmon, "Baroclinic instability and geostrophic turbulence," Geophys. Astrophys. Fluid Dyn. **15**, 167 (1980).
[22] M. Golubitsky, I. Stewart, and D. G. Schaeffer, *Singularities and Groups in Bifurcation Theory* (Springer-Verlag, New York, 1988), vol. 2.
[23] D. Pino, M. Net, J. Sánchez, and I. Mercader, "Thermal Rossby waves in a rotating annulus. their stability," Phys. Rev. E **63**, 056312 (2001).
[24] G. M. Lewis and W. Nagata, "Double Hopf bifurcations in the differentially heated rotating annulus," SIAM J. Appl. Math. **63**, 1029 (2003).
[25] G. M. Lewis and W. Nagata, "Double Hopf bifurcations in the quasigeostrophic potential vorticity equations," Dyn. Contin. Discrete Impulsive Syst.: Ser. B - Appl. Algorithms **12**, 783 (2003).
[26] G. M. Lewis and W. Nagata, "Linear stability analysis for the differentially heated rotating annulus," Geophys. Astrophys. Fluid Dyn. **98**, 129 (2004).
[27] I. Mercader, O. Batiste, and A. Alonso, "Continuation of travelling-wave solutions of the Navier-Stokes equations," Int. J. Numer. Methods Fluids **52**, 707 (2006).
[28] A. A. Castrejón-Pita and P. L. Read, "Baroclinic waves in an air-filled thermally driven rotating annulus," Phys. Rev. E **75**, 026301 (2007).
[29] J. S. Fein and R. L. Pfeffer, "An experimental study of the effects of Prandtl number on thermal convection in a rotating, differentially heated cylindrical annulus of fluid," J. Fluid Mech. **75**, 81 (1976).
[30] P. R. Jonas, "Some effects of boundary conditions and fluid properties on vacillation in thermally driven rotating flow in an annulus," Geophys. Astrophys. Fluid Dyn. **18**, 1 (1981).
[31] W. W. Fowlis and R. Hide, "Thermal convection in a rotating annulus of liquid: effect of viscosity on the transition between axisymmetric and non-axisymmetric flow regimes," J. Atmos. Sci. **22**, 541 (1965).
[32] J. M. Vanel, R. Peyret, and P. Bontoux, in *Numerical Methods in Fluid Dynamics II*, edited by K. W. Morton and M. J. Baines (Clarendon, Oxford, 1986), pp. 463–475.
[33] I. Raspo, S. Hugues, E. Serre, A. Randriamampianina, and P. Bontoux, "A spectral projection method for the simulation of complex three-dimensional rotating flows," Comput. Fluids **31**, 745 (2002).
[34] P. L. Read, "Phase portrait reconstruction using multivariate singular systems analysis," Physica D **69**, 353 (1993).
[35] R. W. Preisendorfer, *Principal Component Analysis in Meteorology and Oceanography* (Elsevier, Amsterdam, 1988).
[36] P. Maubert and A. Randriamampianina, "Transition vers la turbulence géostrophique pour un écoulement d'air en cavité tournante différentiellement chauffée," C. R. Mec. **330**, 365 (2002).
[37] R. Hide, "An experimental study of thermal convection in a rotating fluid," Philos. Trans. R. Soc. London, Ser. A **250**, 441 (1958).
[38] B. J. Hoskins, "The mathematical theory of frontogenesis," Annu. Rev. Fluid Mech. **14**, 131 (1982).
[39] A. Wolf, J. B. Swift, H. L. Swinney, and J. A. Vastano, "Determining Lyapunov exponents from a time series," Physica D **16**, 285 (1985).